Confinement Assembly of ABC Triblock Terpolymers for the High-Yield Synthesis of Janus Nanorings

*Andrea Steinhaus[1], Ramzi Chakroun[1], Markus Müllner[2], Tai-Lam Nghiem[1], Marcus Hildebrandt[1], André H. Gröschel[1,3,]**

[1] Physical Chemistry, University of Duisburg-Essen, 47057 Duisburg, Germany.

[2] Key Centre for Polymers and Colloids, School of Chemistry, and The University of Sydney Nano Institute (Sydney Nano), The University of Sydney, Sydney 2006, New South Wales, Australia.

[3] Center for Nanointegration Duisburg-Essen (CENIDE), University of Duisburg-Essen, 45127 Essen, Germany.

*Email: andre.groeschel@uni-due.de (A.H.G)

ABSTRACT:

Block copolymers are versatile building blocks for the self-assembly of functional nanostructures in bulk and solution. While spheres, cylinders, and bilayer sheets are thermodynamically preferred shapes and frequently observed, ring-shaped nanoparticles are more challenging to realize due to energetic penalties that originate from their anisotropic curvature. Today, a handful of concepts exist that produce core-shell nanorings, while more complex (*e.g.* patchy) nanorings are currently out of reach and have only been predicted theoretically. Here, we demonstrate that confinement assembly of properly designed ABC triblock terpolymers is a general route to synthesize Janus nanorings in high purity. The triblock terpolymer self-assembles in the spherical confinement of nanoemulsion droplets into prolate ellipsoidal microparticles with an axially-stacked lamellar-ring (*lr*)-morphology. We clarified and visualized this complex, yet well-ordered, morphology with transmission electron tomography (ET). Blocks A and C formed stacks of lamellae with the B

microdomain sandwiched in-between as nanorings. Cross-linking of the B-rings allows disassembly of the microparticles into Janus nanorings (JNRs) carrying two strictly separated polymer brushes of A and C on top and bottom. Decreasing the B volume leads to Janus spheres and rods, while an increase of B results in perforated and filled Janus disks. The confinement assembly of ABC triblock terpolymers is a general process that can be extended to other block chemistries and will allow to synthesize a large variety of complex micro- and nanoparticles that inspire studies in self-assembly, interfacial stabilization, colloidal packing, and nanomedicine.

KEYWORDS: 3D confinement; block copolymers; electron tomography; Janus nanoparticles; nanoemulsions, nanorings; self-assembly;

Ring-shaped molecules and toroidal particles fascinate in science and technology with special physical properties assigned to their shape.[1–4] Probably the best known example is the prokaryotic genome – ring-shaped and circular double-stranded DNA – that serve as carriers of the genetic code and that can be transferred between cells due to their small size and distinct shape.[5] While ring-shaped nanostructures are frequently observed in nature, *e.g.*, protein-conducting channels in cell membranes, protofilament structures, and peroxiredoxin proteins,[6–8] synthetic examples on a macromolecular or colloidal level are less common. The main reasons are the unfavorable energy of the curved architecture and the accompanied reduced degree of freedom of closed loops (as compared to linear analogues). Ring-shaped molecules (*e.g.* rotaxanes and polycatenanes) are thus synthesized from intrinsically bent molecules,[9] while macrocyclic polymers and polymer brushes are formed by cyclisation reactions between functional chain ends.[10–12] These synthetic methods have the advantage of molecular control over ring size, but they usually require highly dilute conditions to prevent linear end-to-end coupling.

Strategies to grow colloidal nanorings form the bottom-up could allow versatile and scalable production, but the challenge is to find processes and physicochemical effects that allow to bend building blocks into the ring-shape in high yield and with high quality. Self-assembly of block copolymers is one powerful concept to create nanoparticles with controlled nanoshapes.[13–15] In case of core-shell nanorings, the formation mostly relies on self-assembly of cylinder micelles followed by ring-closure, *e.g.*, by adjusting solvent conditions,[16,17] mechanical sheering,[18] ionic complexation of triblock terpolymers,[19] or liquid crystalline segments.[20,21] The driving force for ring-closure is not very selective and products often consist of a mixture of different shapes. Reducing the number of growth directions *via* confining interfaces or templates has helped to enhance both yield and quality of self-assembled nanorings. In this regard, the spherical

confinement of oil-in-water emulsions has not only become an appealing technique for the scalable fabrication of block copolymer microparticles,[22–29] but it also allows to shape nanorings from gold nanofibers,[30] carbon nanotubes,[31] and block copolymer cylinders.[32,33] Plasmid DNA was used as monodisperse circular template to confine the self-assembly of block copolymer micelles into homogeneous core-shell nanorings.[34] Other confining templates such as surfactant micelles,[35] DNA origami,[36] and 2D interfaces,[37] have aided the formation of various inorganic nanorings,[37–40] which then served as model systems to study shape-depended plasmon resonance,[41–43] or surface-enhanced Raman scattering.[44] Nanorings have further shown promise in photodynamic therapy,[45] as well as cancer therapy due to the higher uptake of circular shapes into cells as compared to disks and slower released rate as compared to spheres.[46]

These and other synthetic examples for nanorings typically result in a core-shell structure with an isotropic shell. Only few exceptions exist that demonstrated a patchy surface, *e.g.* rings with different chemistry on inside and outside (high and low curvature).[12,40] Due to lack of concepts to create anisotropic surfaces, studies involving nanorings usually focused on shape effects.[1–4] In recent years, particles with anisotropic or patchy surfaces have gained increased attention as they display distinctly different properties than isotropic surfaces including directionality, non-closed packing, and enhanced affinity to interfaces (or other particles).[47] Janus particles are the simplest patchy particle with two strictly separated hemispheres, which have been utilized in numerous applications as summarized in a recent comprehensive review.[48] Up to now, Janus nanorings have not been realized so far. To unlock studies on surface anisotropic nanorings, a versatile concept would be desirable for their reliable production.

Here, we show that the combination of confinement conditions and properly designed ABC triblock terpolymers is a general route to synthesize Janus nanorings in high yield and quality. We

chose ABC triblock terpolymers with equal-sized A and C endblocks, and a varying B fraction to form lamella morphologies with potentially B-spheres, -cylinders, and -lamella. We hypothesized that in spherical confinement of drying nanoemulsion droplets, the B-cylinders would be deflected at the high-energy boundary of the curved oil/water interface and forced into ring-closure resulting in a lamella-ring (*lr*) morphology. ABC triblock terpolymers have only received very little attention in confinement assembly,[49–51] although they exhibit a very rich microphase behavior in bulk as demonstrated by Stadler and collegues.[52–56] Simulation studies also predict a plethora of terpolymer morphologies in 3D confinement, not accessible by other current procedures,[57] which further encourages to explore this largely uncharted field.

RESULTS AND DISCUSSIONS

In this study, we investigate the confinement assembly of a series of polystyrene-*block*-polybutadiene-*block*-poly(methyl methacrylate) triblock terpolymers (PS-*b*-PB-*b*-PMMA or SBM) consisting of equal-sized PS and PMMA blocks, while the PB weight fraction, f_B, ranged from 11-40 wt.-% (Table 1). The block lengths were chosen, because all SBM terpolymers formed a lamellar morphology under bulk conditions containing either PB spheres (f_B = 11 wt.-%), PB cylinders (f_B = 13-22 wt.-%), or PB lamellae (f_B = 40 wt.-%) (see Figure S1 of the Supporting Information, SI).

Table 1: Polymer specifics of the used SBM triblock terpolymers

code	P_n S [a]	P_n B [a]	P_n M [a]	f_S [b]	f_B [b]	f_M [b]	M_n [c]
SBM1	310	150	340	43	11	46	74
SBM2	640	300	410	54	13	33	124
SBM3	510	260	260	57	14	28	93
SBM4	560	580	540	40	22	38	143
SBM5	620	1500	570	32	40	28	202

[a] Degree of polymerization of the respective block; [b] Weight fraction of the respective block; [c] Molecular weight in x 10^3 g mol^{-1} as determined through a combination of SEC and ^{1}H-NMR; dispersity $Đ$ < 1.15 for all terpolymers determined by SEC using THF as eluent at a flowrate of 1.0 mL min^{-1} and PS calibration.

The preparative steps to form multicompartment microparticles followed by cross-linking into Janus nanorings (JNRs) are summarized in Scheme 1. Exemplified on SBM2, we first dissolved 10 mg of the triblock terpolymer in 1 mL of $CHCl_3$ (c_P = 10 g·L^{-1}) and stirred the solution overnight for equilibration. We then emulsified the polymer solution in 20 mL of water containing cetyltrimethylammonium bromide (CTAB) surfactant (c_S = 10 g·L^{-1}) by vortex mixing for 1 min followed by passing the dispersion through a filter (Versapor®; pore size 1.2 µm) (Scheme 1b).

Scheme 1: Preparation of multicompartment microparticles and JNRs. a) Chemical structure of SBM. b) Emulsion of SBM/$CHCl_3$ droplets in water stabilized by CTAB. c) Microparticles with *lr*-morphology. d) Cross-linking of the PB double bonds with OsO_4 and disassembly into JNRs.

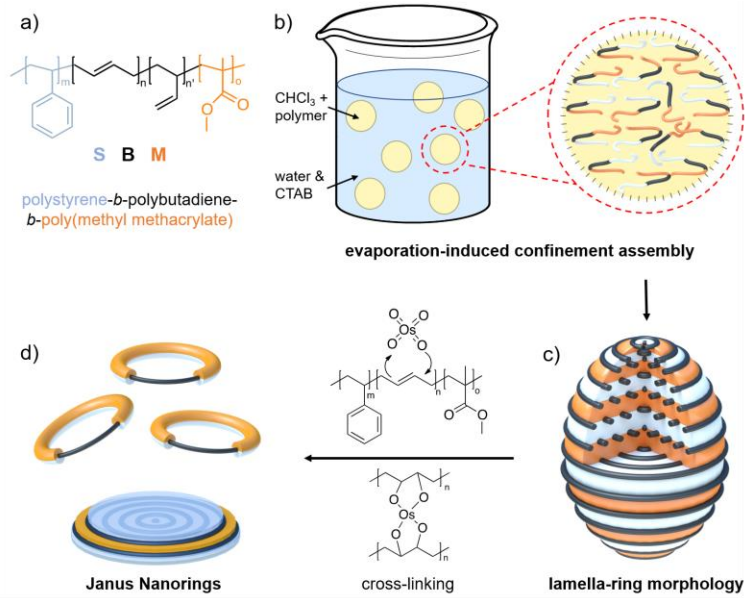

During $CHCl_3$ evaporation, SBM concentrated inside the nanoemulsion droplets and self-assembled into solid multicompartment microparticles. The equal-sized PS/PMMA endblocks arranged into axially-stacked lamellae, in-between which the PB microphase formed a morphology with respect to its weight fraction (Scheme 1c). Finally, we cross-linked the double bonds of the PB microphase to disassemble the microparticles into Janus nanoparticles in a good solvent for all blocks (THF), where we expected JNRs for SBM2-4 (Scheme 1d).

Figure 1a shows the transmission electron microscopy (TEM) overview image of microparticles obtained after confinement self-assembly of SBM2. The size of microparticles ranges from 300-1000 nm with a length to diameter ratio of typically L/D = 1.2-1.6, *i.e.* the microparticles have a prolate elliptic shape. From DLS measurements we obtain a size distribution of R_h = 153 ± 41 nm with $Đ$ = 0.27 (Figure S2). Investigating the inner morphology, three microphases can be clearly distinguished when lamellae align with the viewing direction: two lamellae of PMMA and PS stacking in an alternating manner, and strings of darker PB dots in-between (contrast enhanced with OsO_4) (Figure 1b). PS forms thicker lamellae due to its larger molecular weight and its higher stability under *e*-beam irradiation (greyscale analysis in Figure S3), while PMMA degrades to some extent causing shrinking. It is surprising that we find stacked lamellae instead of concentric ('onion-like') lamellae using only one single surfactant. As shown before for AB diblock copolymers, one block typically has a preferential interaction with the interface resulting in 'onion-like' particles.[58] Stacked lamellae have been observed for surfactant mixtures reducing interfacial tension for both blocks.[29] Recently, we obtained stacked lamellae with single surfactants for diblock molecular polymer brushes,[59] which we attributed to the strong tendency of brushes for planar packing.[60] In our case, PS (δ = 18.5 $MPa^{1/2}$) and PMMA (δ = 19.0 $MPa^{1/2}$) are likely to show comparable affinity towards the CTAB/water interface.[61] If both endblocks seek the

microparticle surface, the ‘onion-like’ arrangement would result in a patchy or mixed PS/PMMA lamella with large unfavorable interface, which can be avoided in form of the stacked lamellae. This hypothesis is further supported by the pronounced corrugation of the surface caused by the periodic necking also visible in scanning electron microscopy (SEM) (Figure S4). By changing the surfactant to polyvinyl alcohol (PVA), we observed spherical microparticles with concentric lamellae, attributed to the difference in polarity of the surfactant and its preferential interaction with the most polar block, PMMA (Figure S5). An alternative explanation could be the fast evaporation of the oil phase, which was recently identified as the cause for axial stacking of lamellae in PS-*b*-PB block copolymer particles prepared from toluene.[28]

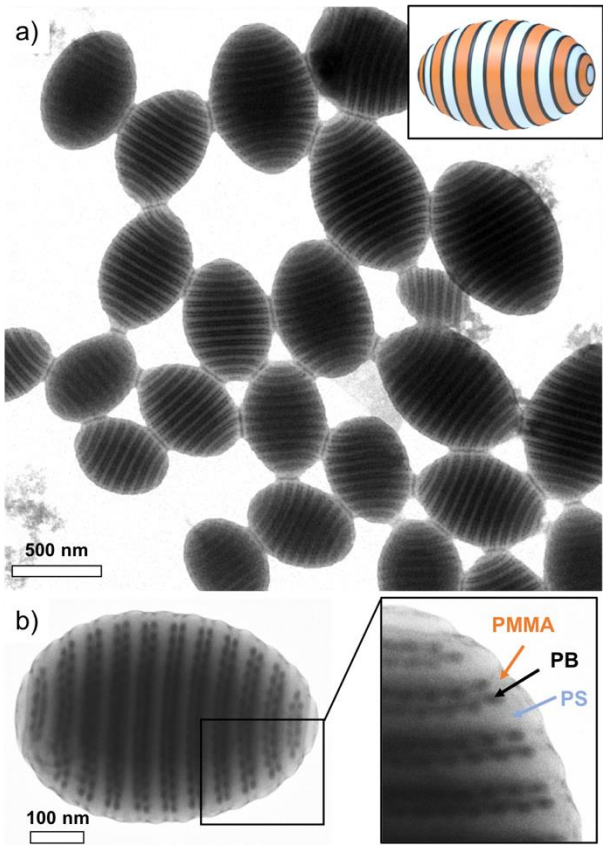

Figure 1: Self-assembly of SBM2 in spherical confinement. a) TEM overview of dried multicompartment microparticles. **b)** Close-up of an individual microparticle showing complex inner nanostructure.

To gain a better understanding of the inner structure, we investigated individual microparticles of SBM2 with electron tomography (Figure 2).[62] Images were taken at varying tilt angles in 3° increments in the range of ± 60° (Figure 2a). When viewed from the side, the PB microphase appears as a dotted line (Figure 2a at 10°), which is expected for a concentric ring layer when viewed along the layer plane (compare Figure S3). When tilted against the long axis of the ellipsoid, PB nanorings became more evident (*e.g.* at $\alpha = 28°$ and $\alpha = 50°$). After image alignment with IMOD software package using gold nanoparticles as fiducial markers we compiled a video (Supporting Video 1) and calculated a 3D reconstruction (Figure 2b).[63] The nanorings are highly ordered judging from frequent observations of overlapping features (lattice fringes) from various viewing angles (Figure S6). These structural features suggest an in-plane (2D) arrangement of concentric PB nanorings that stack in axial direction, which becomes more evident in the video. In the reconstruction, high electron densities are displayed from cold to warm colors allowing us to separate and analyze each layer of PB nanorings individually (Figure 2c). The ring layer closest to the equator of the microparticle consists of the highest number of concentric rings, *n*, (largest diameter of the microparticle). This layer reflects the expected size distribution of JNRs after crosslinking, *i.e.*, the innermost concentric ring is the smallest JNR ($d \approx 50$ nm), while the largest JNR corresponds to the microparticle diameter (*e.g.*, $d = D_h = 300$ nm). In-between these limits all sizes of JNRs will be found. When progressing towards the ellipsoid tips, *n* decreases stepwise (*n*-1) per ring layer. The number of rings in adjacent layers, separated by a PMMA lamella (see blue box in (a)), differs exactly by one (*n*, *n*+1, ...), *e.g.* $n = 4$ rings (green) on top and $n = 5$ rings (red) on bottom. This arrangement allows for an estimation of the overall yield of rings *versus* spheres.

Exemplified on a microparticle species with an average D_h = 306 ± 82 nm, we count in TEM the number of rings *versus* the number of spheres resulting in fraction of rings per microparticle of 86-89 %. In weight, the fraction of rings is even higher and corresponds to a yield of > 99 % (weight fraction of rings per microparticle, see also SI). Overall, the arrangement corresponds to a distorted hexagonal packing of nanorings and originates from an interaction of the PB microphase throughout PS/PMMA lamellae. The concentric arrangement of two rings layers fits into each other as visualized by the green (top) and red (bottom) part. Because of the alternating stacking, the centers of the ring layers alternate between a central PB sphere (green dot) and the smallest possible PB ring (red hole) (Figure 2d). It is energetically unfavorable for the PB microphase to penetrate through the PS/PMMA lamellae, and thus, the PB nanorings could be described as additionally confined within the 2D boundaries of adjacent lamellae (leading to rings instead of a spiral). From a topological point of view this alignment of topological defects (dots and holes) is highly interesting and will be addressed in detail in a separate study.

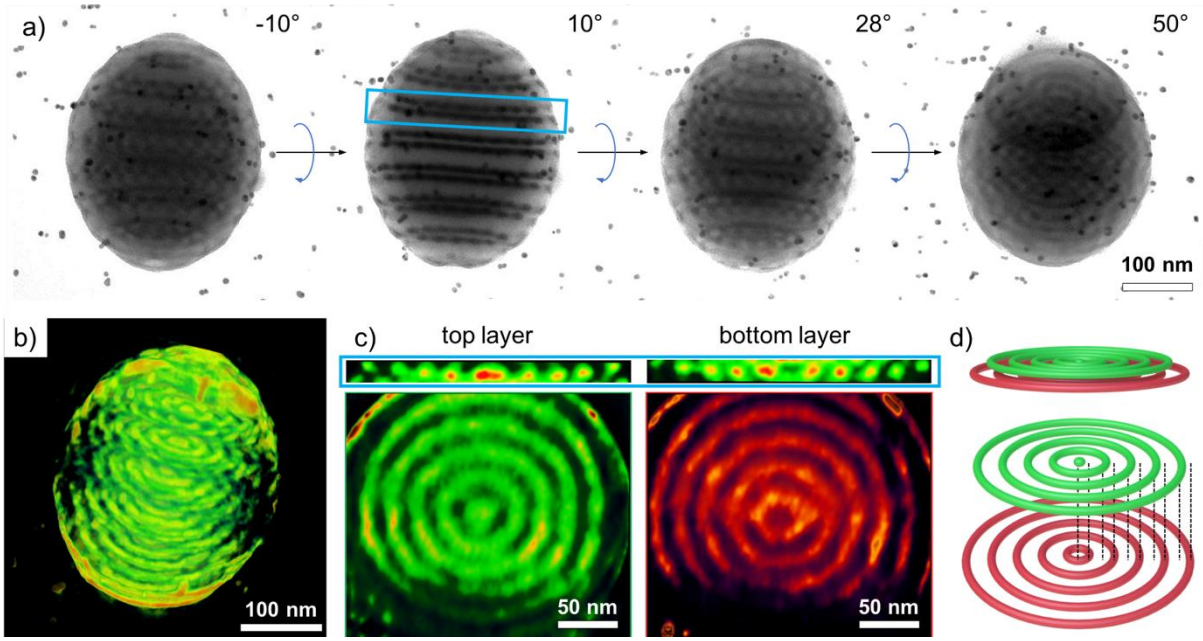

Figure 2: Tomography and reconstruction of SBM2 microparticles. a) Selected images of a TEM tilt-series of an individual multicompartment microparticle. **b)** Tomographic reconstruction of the entire microparticle. **c)** Slice of a double layer of PB nanorings corresponding to the blue box in (a); top layer (green) and bottom layer (red) both consisting of concentric arrangements of PB nanorings. **d)** Schematic clarifying the complementary match of both nanoring layers.

Based on the gathered information from TEM and ET, we can solve the location and arrangement of the polymer blocks within the SBM microparticle (Scheme 2). The particle in Scheme 2a was cropped to visualize the inner morphology that consist of alternating lamellae PS (grey) and PMMA (orange) intercalated with the PB nanorings. The nanorings adopt a 2D concentric arrangement in-between the PS/PMMA lamella. The PS and PMMA chains are entirely separated, but covalently bound to the PB rings (Scheme 2b). Cross-linking of the PB rings permanently fixes the ring-shape and fixes the PS chains on one half and PMMA chains to other half of the nanorings, giving them a Janus character. Since PS and PMMA are only supramolecularly entangled, the *lr*-morphology can be disassembled into individual Janus nanorings in good solvents (Scheme 2c).

Scheme 2: Chain arrangement within the *lr*-morphology. a) Microparticle with axially-stacked *lr*-morphology. b) Strict microphase separation of PS, PB and, PMMA. c) Nanorings with strict separation of PMMA and PS on both sides of the PB core.

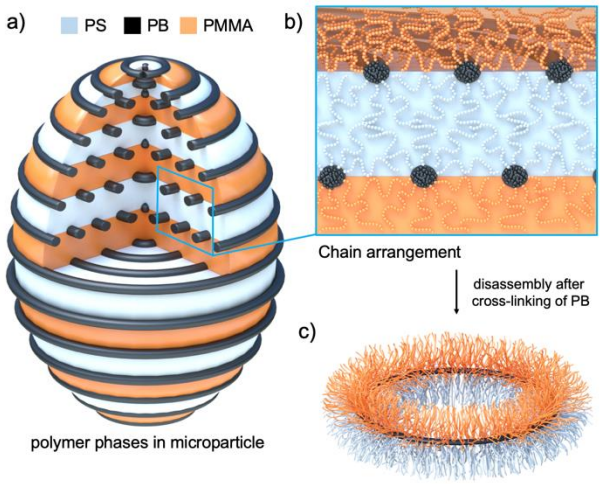

To create and analyze JNRs, we cross-linked the PB microdomain of SBM2 microparticles by addition of aqueous OsO_4 solution to the particle dispersion (Figure 3). OsO_4 migrates into the polymer domains and selectively binds to the PB double bonds.[64] The reaction with two double bonds of different polymer chains fixes the structure and nanorings are liberated after disassembly in THF. Figure 3a shows a SEM image of SBM2 JNRs on a silicon wafer after drying from THF and sputtering with a 2.5 nm layer of Pt. We find ring-shaped nanoparticles with a broad size distribution, which is attributed to the size distribution of microparticles, but also to the natural size distribution of the concentric ring arrangement within each microparticle. The nanorings dried into an intrinsically porous film, where we assign the porosity to the specific ring-shape.

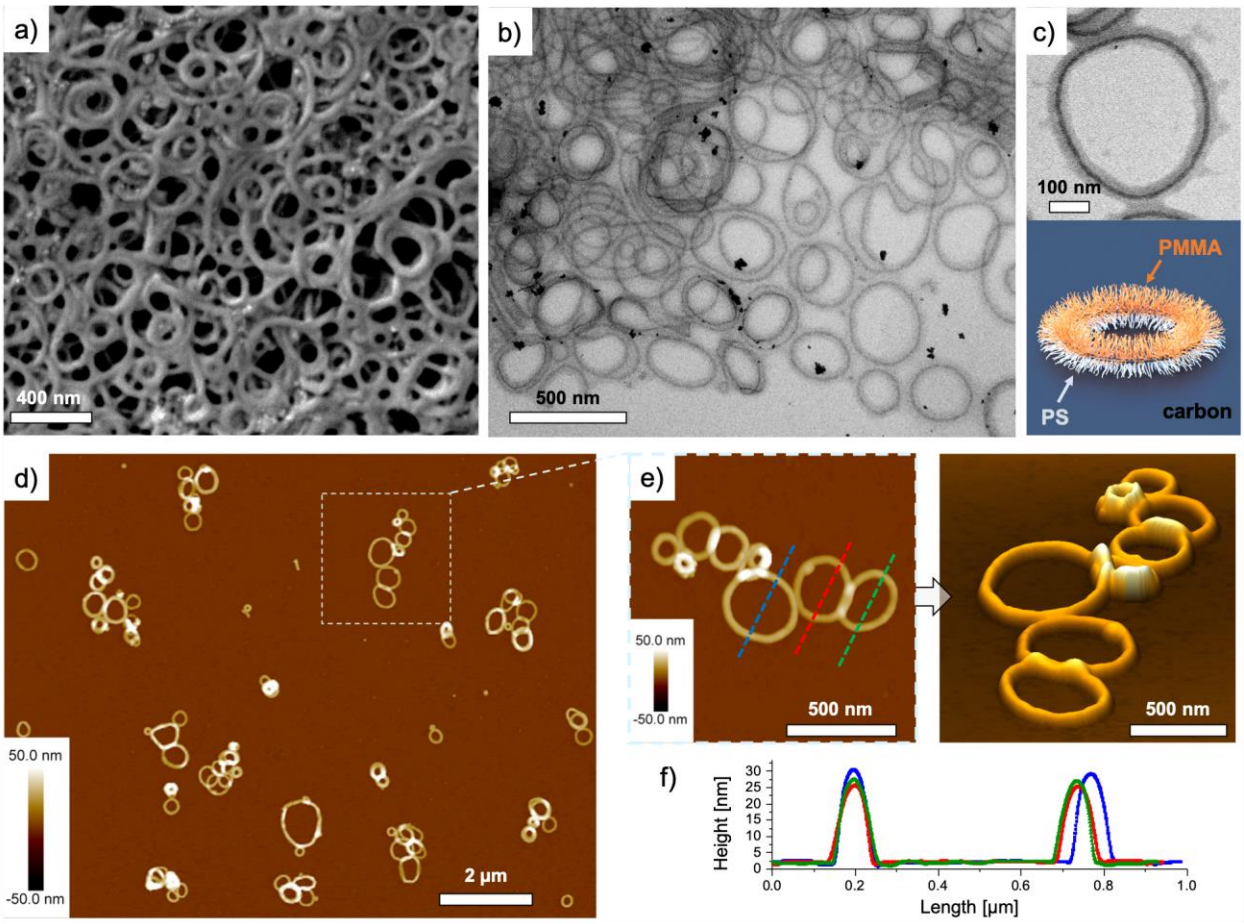

Figure 3: JNRs of SBM2 after cross-linking with OsO_4 and disassembly in THF. a) SEM overview image of JNRs (sputtered with 2.5 nm Pt-layer). **b)** TEM overview image and **c)** close-up of an individual JNRs showing the dark PB core; schematic illustrates arrangement of chains and preferential orientation of JNRs on the carbon film. **d)** AFM overview image of JNRs. **e)** Close-up of an ensemble of JNRs and topographic representation. **f)** Height profile measurements of the colored lines from (e).

The location of polymer microdomains becomes more evident from the TEM overview image in Figure 3b and the close-up in Figure 3c. There, nanorings have a PB core with homogeneous thickness appearing dark from the OsO_4. In previous works on Janus spheres and cylinders, the Janus character could easily be identified when particles were observed from the side (along the Janus axis).[65,66] Due to the ring geometry and ring tension, JNRs always lie flat on the carbon film

of the TEM grid and it is unlikely to distinguish both hemispheres by viewing along the circumference of the JNR. The schematic in Figure 3c illustrates this preferential orientation towards the carbon film. In transmission, the contrast of the shell is always the combined contribution of PMMA and PS, which results in a homogeneous shadow on the in- and outside. The Janus character can be seen in rare cases when particles aggregated during drying or chains dried asymmetrically around the PB core (Figure S7). The AFM overview image (Figure 3d and Figure S8) likewise shows the natural size distribution of JNRs, but reveals that the JNRs have a similar average height of $h \approx$ 25-30 nm, irrespective of the ring size (Figure 3e, f). The height is a result of the low length dispersity of the SBM triblock terpolymers and the well-defined morphology within the microparticle. Overall, this process efficiently produces JNRs in high yield and quality, as all employed SBM terpolymer is converted into Janus nanoparticles, and the fraction of JNRs as compared to other shapes such as Janus cylinders and spheres is very high. In isolated cases, we also observe either broken nanorings (cylinders) or connected loops as well as branched nanorings.

By changing emulsification conditions as well as the block composition, we test system parameters and the limits for JNR formation. We first prepared a series of SBM concentrations ranging from c_P = 1.0 - 50 g·L^{-1} with a fixed surfactant concentration of c_S = 10 g·L^{-1} allowing to increase the overall quantity of JNRs. Measuring the resulting diameter with DLS, we found a linear dependence of the hydrodynamic volume of the microparticles on polymer concentration ($R_h^3 \sim c_P$) (Figure S9a). Neglecting viscosity effects, the diameter of the initial $CHCl_3$ droplets is the same for all polymer concentrations, but after evaporation of $CHCl_3$ more polymer material remained per droplet leading to larger particles. In contrast, employing different syringe filters seemed to have no noticeable effect on the particle size; the obtained diameters remain almost

constant for pore diameter of 0.45 µm, 1.2 µm, and 5 µm (Figure S9b). This suggests that the procedure is rather robust and microparticle diameter can be obtained reproducibly under various conditions.

Finally, we employed SBM terpolymers differing primarily in the PB content to analyze changes to *lr*-morphology (Figure 4; compare also Table 1). Starting with SBM1 and a PB weight fraction of f_B = 11 wt.-%, we record axially-stacked lamellae with seemingly identical *lr*-morphology. However, after cross-linking we did not observe JNRs, but instead Janus nanospheres mixed with short Janus nanorods (Figure 4a). Due to the small f_B, the *lr*-morphology cannot fully develop in the microparticle and instead, short rods and spheres developed as fragments of the nanorings. This observation suggests that the PB microdomains are spheres arranged in concentric circles. At a critical f_B the PB spheres overlap and form PB rings. SBM2 with f_B = 13 wt.-% has already been described above (Figure 4b). At this f_B, nanorings appear flexible judging from the various bending and twisting modes (Figure S10). The PB core of the JNRs does not seem to have a continuous thickness (undulating), which further supports the hypothesis of a morphological evolution from PB spheres to rings. Upon further increase to f_B = 14 wt.-% (SBM3), while decreasing the molecular weight and the PMMA/PS ratio from 1.6 to 1.9 (asymmetry), we still found both the *lr*-morphology within the microparticles and JNRs after crosslinking. This demonstrates that the *lr*-morphology tolerates deviation from entirely symmetric end blocks. Aside from very few Janus cylinders, we almost exclusively find JNRs (see also Figure S11). In AFM we determine an average height of $h \approx$ 15-20 nm for JNRs of SBM3, which is thinner as compared to SBM2 due to the lower overall molecular weight. When increasing the PB domain to f_B = 22 wt.-% (SBM4) as well as the molecular weight, we still observed the *lr*-morphology (Supporting Video 2 and Figure 4c). The produced JNRs of SBM4 have a thicker more pronounced core, they are less flexible, and

show an increased average height in AFM ($h \approx$ 30-35 nm). Aside from JNRs we observed Janus disks with a variety of perforated patterns of the core as transition nanostructures (see also parallel stripes in Figure S12). At 22 wt.-%, the PB microphase of the microparticle seems to be close to a structural transition from concentric rings to perforated disks *via* fusion of PB rings between the PS/PMMA lamellae. This transition might be further enhanced by the volume increase during cross-linking explaining why we still clearly identify the *lr*-morphology before cross-linking. As the preparation conditions and chain arrangements are otherwise identical, the Janus character should still be retained. The perforations are reminiscent of previously reported Janus sheets obtained from bulk morphologies.[67] As f_B was increased further to 40 wt.-%, the PB microphase formed a continuous lamella (PS/PB/PMMA lamella-lamella morphology) resulting in completely filled Janus disks after cross-linking (Figure 4d). Janus disks had been prepared before from AB diblock copolymers in confinement using specific block chemistries and cross-linking protocols,[68] but we expect ABC triblock terpolymers to be a more versatile system for the synthesis and modification of Janus disks (*e.g.* variable block chemistries and tunable thickness). With increasing f_B = 11-40 wt.-%, the microparticles become more anisotropic, which we believe to originate from anisotropic chain stretching at the interface of the PB microdomain. While small PB-spheres (f_B = 11 wt.-%) provide PS/PMMA chains with space to coil (high curvature of PB microdomain), less space is available the interface of PB-rings due to tighter chain packing (lower curvature). In case of f_B = 40 wt.-%, the PB-lamella causes densest chain packing at the PB/PS and PB/PMMA interface enhancing chain stretching of both PS and PMMA. This anisotropy of chain stretching then translates into the observed anisotropy of the microparticle.

Overall, the relationship between increasing f_B in the SBM terpolymer and the resulting Janus nanostructures shows a relatively narrow window to obtain JNRs, but it also shows that a larger

variety of potential Janus nanostructures is hidden in confinement than expected. We are currently studying the filling of nanorings to disks in a series of experiments by gradually increasing the PB volume fraction.

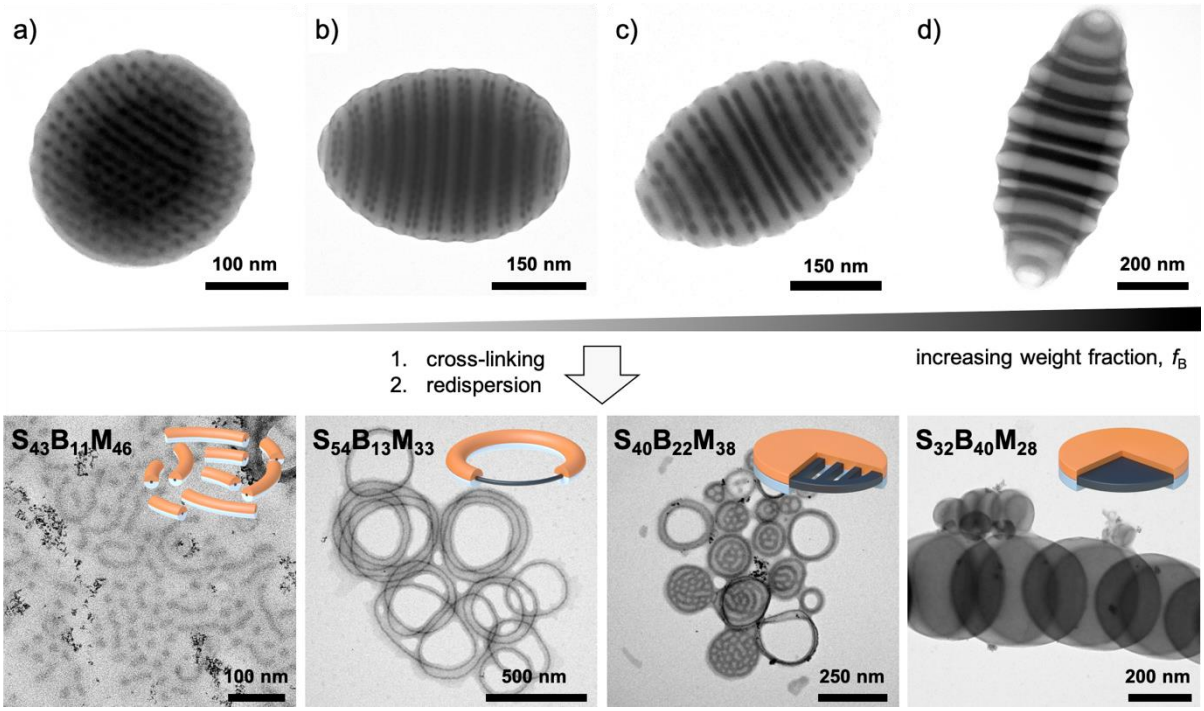

Figure 4: Effect of PB weight fraction on microstructure and Janus nanoparticles. a) SBM1 with f_B = 11 wt.-%, **b)** SBM2 with f_B = 13 wt.-%, **c)** SBM4 with f_B = 22 wt.-%, and **d)** SBM5 with f_B = 40 wt.-%.

CONCLUSION

In summary, we have shown that the self-assembly of ABC triblock terpolymers in spherical confinement is a versatile route to synthesize JNRs. Nanorings in general may find use for fundamental studies of physical properties of cyclic brushes,[12] as building block for intrinsically porous materials,[17] and in delivery applications *(e.g.* as compared to cylindrical nanoparticles).[46] The ring-shape and the Janus properties may in combination be used as colloidal surfactants in applications where stabilization of interfaces is relevant, *e.g.*, as compatibilizers, emulsifiers, and

dispersants.[69–72] Depending on the ring stiffness, this geometry could lead to intrinsically perforated coatings on surfaces and droplet interfaces. The presented investigations indicate a complex morphological behavior of ABC triblock terpolymers in confinement. Considering the potential of available triblock terpolymers, a large number of complex morphologies should become accessible useful to create functional microparticles and nanoparticles.

METHODS

Materials. All chemicals were used as received unless stated otherwise. Cetyltrimethylammonium bromide (CTAB, >99%) and polyvinyl alcohol (PVA, M_n = 13-23 kg·mol^{-1}, 87-89%) were received from Sigma-Aldrich. Ultrapure water was obtained from a Milli-Q® Integral Water Purification System and used for the preparation of emulsions and purification. As dialysis tube a cellulose membrane was used with an average flat width of 33 mm and a MWCO of 12-14 kDa (Sigma Aldrich). The PS-*b*-PB-*b*-PMMA triblock terpolymers were synthetized by sequential anionic polymerization as describe before elsewhere.[73]

Preparation of SBM bulk films. To prepare reference bulk morphologies, 100 mg of terpolymer was dissolved in 2 mL $CHCl_3$ in a 40 mL glass vial. The solvent was evaporated over the course of 6 days under constant $CHCl_3$ atmosphere. After film formation, the vial was cooled with liquid nitrogen and the bulk film was released by breaking the vial. For TEM measurements, bulk films were cut into ultrathin sections on a Leica EM UC7 ultramicrotome, deposited on a carbon-coated copper grid (200 mesh, Science Services), and stained with OsO_4 vapor for 2 h prior to measurements.

Preparation of SBM nanoemulsion droplets. An aqueous stock solution of CTAB (10 g·L^{-1}) was prepared by dissolving the surfactant in Millipore water while heating. The SBM triblock terpolymer was dissolved in $CHCl_3$ at a concentration of 10 g·L^{-1}. In a 40 ml vial, 1 mL of polymer

solution was mixed with 20 mL of CTAB solution and vortexed for 1 min. Emulsification was supported by passing the emulsion through a syringe filter with pore sizes of 0.45, 1.2, and 5 µm (Versapor®). Thereafter, the solvent was evaporated in open vials for 3 days at room temperature.

Purification Process. The microparticle dispersion was transferred to a dialysis tube and excess surfactant removed by dialysis into ultrapure water. Samples were put in a 2 L beaker, which was changed at least 4 times before the particle dispersion was stored in a 40 mL vial. The final particle concentration was about 0.5 $g \cdot L^{-1}$.

Cross-linking of PB domains. In a 2 mL vial 200 µl of the purified microparticle dispersion was mixed with aqueous OsO_4 solution (4 wt.-%) (25.5 µl per 1 mg of polymer; PB/OsO_4 1:1). The dispersion was stirred for 2 hours at room temperature in a closed vial. To remove excess and unreacted OsO_4, the cap was removed and stirring was continued overnight, followed by three centrifugation cycles (6000 rpm, 20 min) and redispersion of the residue in ultrapure water. After the last centrifugation cycle, the residue was dispersed in THF, which allows the full solvation of the PS and PMMA domain, whereas the PB domain remains fixed from the cross-linking.

Nuclear magnetic resonance (^{1}H-NMR) spectra of the samples were recorded on a Bruker DMX300 (300 MHz) spectrometer with $CDCl_3$ as solvent.

Size-exclusion chromatography (SEC). The determination of the molecular weight distributions and polydispersity index of all polymers was conducted on a 1260 Infinity (Polymer Standard Service, Mainz) instrument equipped with 3 SDV columns (pore sizes 10^3, 10^5, 10^6 Å) and a refractive index detector. HPLC grade THF was used as eluent and the samples were eluted at a flow rate of 1.0 mL min^{-1} and 40 °C. For calibration, a narrow molecular weight polystyrene standard kit (Polymer Standard Service, Mainz) was used together with the WinGPC UniChrom software.

Atomic force microscopy (AFM). AFM imaging was performed in air using a Veeco Dimension 5000 with NanoScope V controller and tapping-mode cantilevers (35 Nm^{-1}, RFESP-190, Bruker). AFM specimen were prepared by drop-casting a solution of cross-linked and dispersed JNRs (0.5 $g \cdot L^{-1}$, in THF) on a freshly cleaved mica plate and subsequently dry-blowing using a stream of nitrogen. Images were processed with Bruker Nanoscope software.

Dynamic light scattering (DLS). Measurements were conducted on a LS Instruments spectrometer operated with a Nd:YAG solid state laser (max. 100 mW constant power output at λ = 660 nm). Samples were prepared with concentrations of 0.1 $g \cdot L^{-1}$ and purified from dust by passing the solutions through a PTFE filter of 5 µm pore size directly into dust-free cylindrical quartz cuvettes (diameter 10 mm). Three intensity-time autocorrelation functions were averaged at a scattering angle of 90° with an acquisition time of 60 seconds. The recorded data was analyzed with LS spectrometer v.63 software package.

Transmission electron microscopy (TEM). Measurements were performed on a JEOL JEM-1400 Plus TEM, operating at an accelerating voltage of 120 kV, a point resolution of 0.38 nm as well as a line resolution of 0.2 nm. Images were recorded with 16-bit 4096×4096 Pixel CMOS digital camera and processed FIJI open-source software package.[74] For sample preparation, one drop of the particle dispersion (c = 0.5 $g \cdot L^{-1}$) was deposited on a carbon-coated copper grid (200 mesh, Science Services). All samples were stained with OsO_4 vapor for 3 h prior to measurements.

TEM tomography (ET). Tilt series of microparticles were acquired between ±60° in 3° increments with the SerialEM software package (version 3.2.2). For image alignment purposes, the TEM grids were dipped in gold nanoparticle (fiducial markers) solution before sample deposition (d = 10-15 nm, stabilized by dodecane thiol ligand). Pre-alignment of tilt image series was done with IMOD.[63] Volumetric graphics and analyses were performed with the UCSF Chimera

package and low-pass filtered with Chimera's Gaussian filter with 3.0 voxel radius.[75] The supporting video 1 and 2 was compiled after alignment using Fiji.

Scanning electron microscopy (SEM). Measurements were performed on a cryo-field emission SEM equipped with in lens-, chamber-, and energy-selective detectors for 16 Bit image series acquisition with up to 40,000×50,000-pixel resolution. Samples for SEM measurements were prepared by putting one drop of an approximately 0.1 $g \cdot L^{-1}$ sample dispersion on a mica wafer. After 30 s the solution was blotted with a paper tissue and the wafer was dried for at least 12 h. Afterwards a layer of 2-3 nm was sputtered on the samples using a Quorum PP3010T-Cryo chamber with integrated Q150T-Es high-end sputter coater and Pt-Cd target.

ASSOCIATED CONTENT

Supporting Information

The Supporting Information is available free of charge on the ACS Publications website. The Supporting Figures S1−S12 contain TEM images of terpolymer bulk films, DLS size distributions of microparticles, TEM grey scale analysis of the microparticle morphology, TEM and SEM overview images of microparticles, TEM and AFM overview images of JNRs, and variation of particle sizes with preparation conditions. The authors declare no competing financial interest.

AUTHOR INFORMATION

Corresponding Author

*Email (A.H. Gröschel): andre.groeschel@uni-due.de

Author Contributions

AS performed all experiments except AFM, which was done by MM and MH, RC performed DLS measurements and TLN aided in ET. The manuscript was jointly written by AS and AHG. All authors discussed results, commented on the manuscript, and have given approval to the final version of the manuscript. AHG conceived and supervised the project.

ACKNOWLEDGMENT

The authors acknowledge the Imaging Centre Essen (IMCES) at the University Clinic Essen where the TEM data was recorded. AHG, AS, and TLN acknowledge support from Evonik industries and the German Research Foundation (DFG) through the Emmy Noether Program (No. 376920678). MM is grateful for the support received the ARC Discovery Early Career Researcher Award (DE180100007) and the Australian Nanotechnology Network Overseas Travel Fellowship. MM made use of the Aalto University Nanomicroscopy Center (Aalto-NMC) premises.

REFERENCES

(1) Manoharan, V. N. Colloidal Matter: Packing, Geometry, and Entropy. *Science* **2015**, *349*, 1253751–1253751.

(2) Williams, R. J.; Dove, A. P.; O'Reilly, R. K. Self-Assembly of Cyclic Polymers. *Polym. Chem.* **2015**, *6*, 2998–3008.

(3) Senyuk, B.; Liu, Q.; He, S.; Kamien, R. D.; Kusner, R. B.; Lubensky, T. C.; Smalyukh, I. I. Topological Colloids. *Nature* **2012**, *493*, 200–205.

(4) Avendaño, C.; Jackson, G.; Müller, E. A.; Escobedo, F. A. Assembly of Porous Smectic Structures Formed from Interlocking High-Symmetry Planar Nanorings. *Proc. Natl. Acad. Sci. U. S. A.* **2016**, *113*, 9699–9703.

(5) Richmond, M. H. Bacterial Plasmids. *Biochem. Educ.* **1974**, *2*, 17.

(6) Wang, H.-W.; Chen, Y.; Yang, H.; Chen, X.; Duan, M.-X.; Tai, P. C.; Sui, S.-F. Ring-like Pore Structures of SecA: Implication for Bacterial Protein-Conducting Channels. *Proc. Natl. Acad. Sci. U. S. A.* **2003**, *100*, 4221–4226.

(7) Adams, D. W.; Errington, J. Bacterial Cell Division: Assembly, Maintenance and Disassembly of the Z Ring. *Nat. Rev. Microbiol.* **2009**, *7*, 642–653.

(8) Yewdall, N. A.; Allison, T. M.; Pearce, F. G.; Robinson, C. V.; Gerrard, J. A. Self-Assembly of Toroidal Proteins Explored Using Native Mass Spectrometry. *Chem. Sci.* **2018**, *9*, 6099–6106.

(9) Wu, Q.; Rauscher, P. M.; Lang, X.; Wojtecki, R. J.; de Pablo, J. J.; Hore, M. J. A.; Rowan, S. J. Poly[n]Catenanes: Synthesis of Molecular Interlocked Chains. *Science* **2017**, *358*, 1434–1439.

(10) Kim, Y.; Li, W.; Shin, S.; Lee, M. Development of Toroidal Nanostructures by Self-Assembly: Rational Designs and Applications. *Acc. Chem. Res.* **2013**, *46*, 2888–2897.

(11) Zhang, S.; Tezuka, Y.; Zhang, Z.; Li, N.; Zhang, W.; Zhu, X. Recent Advances in the Construction of Cyclic Grafted Polymers and Their Potential Applications. *Polym. Chem.* **2018**, *9*, 677–686.

(12) Schappacher, M.; Deffieux, A. Synthesis of Macrocyclic Copolymer Brushes and Their Self-Assembly into Supramolecular Tubes. *Science* **2008**, *319*, 1512–1515.

(13) Schacher, F. H.; Rupar, P. A.; Manners, I. Functional Block Copolymers: Nanostructured Materials with Emerging Applications. *Angew. Chemie Int. Ed.* **2012**, *51*, 7898–7921.

(14) Gröschel, A. H.; Müller, A. H. E. Self-Assembly Concepts for Multicompartment Nanostructures. *Nanoscale* **2015**, *7*, 11841–11876.

(15) Chen, C.; Wylie, R. A. L.; Klinger, D.; Connal, L. A. Shape Control of Soft Nanoparticles and Their Assemblies. *Chem. Mater.* **2017**, *29*, 1918–1945.

(16) Yang, C.; Gao, L.; Lin, J.; Wang, L.; Cai, C.; Wei, Y.; Li, Z. Toroid Formation through a Supramolecular "Cyclization Reaction" of Rodlike Micelles. *Angew. Chemie - Int. Ed.* **2017**, *56*, 5546–5550.

(17) Cai, J.; Mineart, K. P.; Li, X.; Spontak, R. J.; Manners, I.; Qiu, H. Hierarchical Self-Assembly of Toroidal Micelles into Multidimensional Nanoporous Superstructures. *ACS Macro Lett.* **2018**, 1040–1045.

(18) Yu, H.; Jiang, W. Effect of Shear Flow on the Formation of Ring-Shaped Aba Amphiphilic Triblock Copolymer Micelles. *Macromolecules* **2009**, *42*, 3399–3404.

(19) Pochan, D. J.; Chen, Z.; Cui, H.; Hales, K.; Qi, K.; Wooley, K. L. Toroidal Triblock Copolymer Assemblies. *Science* **2004**, *306*, 94–97.

(20) Kim, J. K.; Lee, E.; Huang, Z.; Lee, M. Nanorings from the Self-Assembly of Amphiphilic Molecular Dumbbells. *J. Am. Chem. Soc.* **2006**, *128*, 14022–14023.

(21) Li, X.; Gao, Y.; Xing, X.; Liu, G. Polygonal Micellar Aggregates of a Triblock Terpolymer Containing a Liquid Crystalline Block. *Macromolecules* **2013**, *46*, 7436–7442.

(22) Wyman, I.; Njikang, G.; Liu, G. When Emulsification Meets Self-Assembly: The Role of

Emulsification in Directing Block Copolymer Assembly. *Prog. Polym. Sci.* **2011**, *36*, 1152–1183.

(23) Yabu, H.; Higuchi, T.; Jinnai, H. Frustrated Phases: Polymeric Self-Assemblies in a 3D Confinement. *Soft Matter* **2014**, *10*, 2919.

(24) Jang, S. G.; Audus, D. J.; Klinger, D.; Krogstad, D. V; Kim, B. J.; Cameron, A.; Kim, S.; Delaney, K. T.; Hur, S.; Killops, K. L.; Fredrickson, G. H.; Kramer, E. J.; Hawker, C. J. Striped, Ellipsoidal Particles by Controlled Assembly of Diblock Copolymers. *J. Am. Chem. Soc.* **2013**, *135*, 6649–6657.

(25) Ku, K. H.; Shin, J. M.; Klinger, D.; Jang, S. G.; Hayward, R. C.; Hawker, C. J.; Kim, B. J. Particles with Tunable Porosity and Morphology by Controlling Interfacial Instability in Block Copolymer Emulsions. *ACS Nano* **2016**, *10*, 5243–5251.

(26) Higuchi, T.; Tajima, A.; Motoyoshi, K.; Yabu, H.; Shimomura, M. Suprapolymer Structures from Nanostructured Polymer Particles. *Angew. Chemie Int. Ed.* **2009**, *48*, 5125–5128.

(27) Shin, J. M.; Kim, M. P.; Yang, H.; Ku, K. H.; Jang, S. G.; Youm, K. H.; Yi, G. R.; Kim, B. J. Monodipserse Nanostructured Spheres of Block Copolymers and Nanoparticles *via* Cross-Flow Membrane Emulsification. *Chem. Mater.* **2015**, *27*, 6314–6321.

(28) Shin, J. M.; Kim, Y.; Yun, H.; Yi, G.-R.; Kim, B. J. Morphological Evolution of Block Copolymer Particles: Effect of Solvent Evaporation Rate on Particle Shape and Morphology. *ACS Nano* **2017**, *11*, 2133–2142.

(29) Klinger, D.; Wang, C. X.; Connal, L. A.; Audus, D. J.; Jang, S. G.; Kraemer, S.; Killops, K. L.; Fredrickson, G. H.; Kramer, E. J.; Hawker, C. J. A Facile Synthesis of Dynamic, Shape-Changing Polymer Particles. *Angew. Chemie Int. Ed.* **2014**, *53*, 7018–7022.

(30) Chen, Y.; Wang, Y.; Peng, J.; Xu, Q.; Weng, J.; Xu, J. Assembly of Ultrathin Gold Nanowires: From Polymer Analogue to Colloidal Block. *ACS Nano* **2017**, *11*, 2756–2763.

(31) Chen, L.; Yu, S.; Wang, H.; Xu, J.; Liu, C.; Chong, W. H.; Chen, H. General Methodology of Using Oil-in-Water and Water-in-Oil Emulsions for Coiling Nanofilaments. *J. Am. Chem. Soc.* **2013**, *135*, 835–843.

(32) Yabu, H.; Sato, S.; Higuchi, T.; Jinnai, H.; Shimomura, M. Creating Suprapolymer Assemblies: Nanowires, Nanorings, and Nanospheres Prepared from Symmetric Block-Copolymers Confined in Spherical Particles. *J. Mater. Chem.* **2012**, *22*, 7672.

(33) Jia, Z.; Bobrin, V. A.; Monteiro, M. J. Temperature-Directed Assembly of Stacked Toroidal Nanorattles. *ACS Macro Lett.* **2017**, 1223–1227.

(34) Zhang, K.; Miao, H.; Chen, D. Water-Soluble Monodisperse Core-Shell Nanorings: Their Tailorable Preparation and Interactions with Oppositely Charged Spheres of a Similar Diameter. *J. Am. Chem. Soc.* **2014**, *136*, 15933–15941.

(35) Yan, Y.; Padmanabha Pillai, P.; Timonen, J. V. I.; Emami, F. S.; Vahid, A.; Grzybowski, B. A. Synthesis of Toroidal Gold Nanoparticles Assisted by Soft Templates. *Langmuir* **2014**, *30*, 9886–9890.

(36) Urban, M. J.; Dutta, P. K.; Wang, P.; Duan, X.; Shen, X.; Ding, B.; Ke, Y.; Liu, N. Plasmonic Toroidal Metamolecules Assembled by DNA Origami. *J. Am. Chem. Soc.* **2016**, *138*, 5495–5498.

(37) McLellan, J. M.; Geissler, M.; Xia, Y. Edge Spreading Lithography and Its Application to the Fabrication of Mesoscopic Gold and Silver Rings. *J. Am. Chem. Soc.* **2004**, *126*, 10830–10831.

(38) Zhong, K.; Li, J.; Liu, L.; Brullot, W.; Bloemen, M.; Volodin, A.; Song, K.; Van Dorpe, P.; Verellen, N.; Clays, K. Direct Fabrication of Monodisperse Silica Nanorings from Hollow Spheres – A Template for Core–Shell Nanorings. *ACS Appl. Mater. Interfaces* **2016**, *8*, 10451–10458.

(39) Liusman, C.; Li, S.; Chen, X.; Wei, W.; Zhang, H.; Schatz, G. C.; Boey, F.; Mirkin, C. A. Free-Standing Bimetallic Nanorings and Nanoring Arrays Made by on-Wire Lithography. *ACS Nano* **2010**, *4*, 7676–7682.

(40) Wu, Y.; Luo, Z.; Liu, B.; Yang, Z. Colloidal Rings by Site-Selective Growth on Patchy Colloidal Disc Templates. *Angew. Chemie Int. Ed.* **2017**, *56*, 9807–9811.

(41) Tsai, C. Y.; Lin, J. W.; Wu, C. Y.; Lin, P. T.; Lu, T. W.; Lee, P. T. Plasmonic Coupling in Gold Nanoring Dimers: Observation of Coupled Bonding Mode. *Nano Lett.* **2012**, *12*, 1648–1654.

(42) Halpern, A. R.; Corn, R. M. Lithographically Patterned Electrodeposition of Gold, Silver, and Nickel Nanoring Arrays with Widely Tunable Near-Infrared Plasmonic Resonances. *ACS Nano* **2013**, *7*, 1755–1762.

(43) Lin, X.; Liu, Y.; Lin, M.; Zhang, Q.; Nie, Z. Synthesis of Circular and Triangular Gold Nanorings with Tunable Optical Properties. *Chem. Commun.* **2017**, *53*, 10765–10767.

(44) Banaee, M. G.; Crozier, K. B. Gold Nanorings as Substrates for Surface-Enhanced Raman Scattering. *Opt. Lett.* **2010**, *35*, 760.

(45) Hu, Y.; Yang, Y.; Wang, H.; Du, H. Synergistic Integration of Layer-by-Layer Assembly of Photosensitizer and Gold Nanorings for Enhanced Photodynamic Therapy in the Near Infrared. *ACS Nano* **2015**, *9*, 8744–8754.

(46) Liu, Y.; Wang, Z.; Liu, Y.; Zhu, G.; Jacobson, O.; Fu, X.; Bai, R.; Lin, X.; Lu, N.; Yang, X.; Fan, W.; Song, J.; Wang, Z.; Yu, G.; Zhang, F.; Kalish, H.; Niu, G.; Nie, Z.; Chen, X. Suppressing Nanoparticle-Mononuclear Phagocyte System Interactions of Two-Dimensional Gold Nanorings for Improved Tumor Accumulation and Photothermal Ablation of Tumors. *ACS Nano* **2017**, *11*, 10539–10548.

(47) Ravaine, S.; Duguet, E. Synthesis and Assembly of Patchy Particles: Recent Progress and Future Prospects. *Curr. Opin. Colloid Interface Sci.* **2017**, *30*, 45–53.

(48) Walther, A.; Müller, A. H. E. Janus Particles: Synthesis, Self-Assembly, Physical Properties, and Applications. *Chem. Rev.* **2013**, *113*, 5194–5261.

(49) Zhang, K.; Gao, L.; Chen, Y.; Yang, Z. Onion-like Microspheres with Tricomponent from Gelable Triblock Copolymers. *J. Colloid Interface Sci.* **2010**, *346*, 48–53.

(50) Xu, J.; Wang, K.; Li, J.; Zhou, H.; Xie, X.; Zhu, J. ABC Triblock Copolymer Particles with Tunable Shape and Internal Structure through 3D Confined Assembly. *Macromolecules* **2015**, *48*, 2628–2636.

(51) Xu, J.; Yang, Y.; Wang, K.; Li, J.; Zhou, H.; Xie, X.; Zhu, J. Additives Induced Structural Transformation of ABC Triblock Copolymer Particles. *Langmuir* **2015**, *31*, 10975–10982.

(52) Bates, F. S.; Fredrickson, G. H. Block Copolymers—Designer Soft Materials. *Phys. Today* **1999**, *52*, 32–38.

(53) Stadler, R.; Auschra, C.; Beckmann, J.; Krappe, U.; Voight-Martin, I.; Leibler, L. Morphology and Thermodynamics of Symmetric Poly(A-Block-B-Block-C) Triblock Copolymers. *Macromolecules* **1995**, *28*, 3080–3097.

(54) Abetz, V.; Stadler, R. ABC and BAC Triblock Copolymers - Morphological Engineering by Variation of the Block Sequence. *Macromol. Symp.* **1997**, *113*, 19–26.

(55) Breiner, U.; Krappe, U.; Jakob, T.; Abetz, V.; Stadler, R. Spheres on Spheres - a Novel Spherical Multiphase Morphology in Polystyrene-Block-Polybutadiene-Block-Poly(Methyl Methacrylate) Triblock Copolymers. *Polym. Bull.* **1998**, *40*, 219–226.

(56) Breiner, U.; Krappe, U.; Abetz, V.; Stadler, R. Cylindrical Morphologies in Asymmetric ABC Triblock Copolymers. *Macromol. Chem. Phys.* **1997**, *198*, 1051–1083.

(57) Yan, N.; Zhu, Y.; Jiang, W. Self-Assembly of ABC Triblock Copolymers under 3D Soft Confinement: A Monte Carlo Study. *Soft Matter* **2016**, *12*, 965–972.

(58) Li, L.; Matsunaga, K.; Zhu, J.; Higuchi, T.; Yabu, H.; Shimomura, M.; Jinnai, H.; Hayward, R. C.; Russell, T. P. Solvent-Driven Evolution of Block Copolymer Morphology under 3D Confinement. *Macromolecules* **2010**, *43*, 7807–7812.

(59) Steinhaus, A.; Pelras, T.; Chakroun, R.; Gröschel, A. H.; Müllner, M. Self-Assembly of Diblock Molecular Polymer Brushes in the Spherical Confinement of Nanoemulsion Droplets. *Macromol. Rapid Commun.* **2018**, 1800177.

(60) Pelras, T.; Mahon, C. S.; Müllner, M. Synthesis and Applications of Compartmentalised Molecular Polymer Brushes. *Angew. Chemie Int. Ed.* **2018**, *57*, 6982–6994.

(61) Abetz, V.; Goldacker, T. Formation of Superlattices *via* Blending of Block Copolymers.

Macromol. Rapid Commun. **2000**, *21*, 16–34.

(62) Jinnai, H.; Jiang, X. Electron Tomography in Soft Materials. *Curr. Opin. Solid State Mater. Sci.* **2013**, *17*, 135–142.

(63) Kremer, J. R.; Mastronarde, D. N.; McIntosh, J. R. Computer Visualization of Three-Dimensional Image Data Using IMOD. *J. Struct. Biol.* **1996**, *116*, 71–76.

(64) Higuchi, T.; Tajima, A.; Motoyoshi, K.; Yabu, H.; Shimomura, M. Frustrated Phases of Block Copolymers in Nanoparticles. *Angew. Chemie Int. Ed.* **2008**, *47*, 8044–8046.

(65) Wolf, A.; Walther, A.; Müller, A. H. E. Janus Triad: Three Types of Nonspherical, Nanoscale Janus Particles from One Single Triblock Terpolymer. *Macromolecules* **2011**, *44*, 9221–9229.

(66) Gröschel, A. H.; Walther, A.; Löbling, T. I.; Schmelz, J.; Hanisch, A.; Schmalz, H.; Müller, A. H. E. Facile, Solution-Based Synthesis of Soft, Nanoscale Janus Particles with Tunable Janus Balance. *J. Am. Chem. Soc.* **2012**, *134*, 13850–13860.

(67) Hiekkataipale, P.; Löbling, T. I.; Poutanen, M.; Priimagi, A.; Abetz, V.; Ikkala, O.; Gröschel, A. H. Controlling the Shape of Janus Nanostructures through Supramolecular Modification of ABC Terpolymer Bulk Morphologies. *Polymer* **2016**, *107*, 456–465.

(68) Deng, R.; Liang, F.; Zhou, P.; Zhang, C.; Qu, X.; Wang, Q.; Li, J.; Zhu, J.; Yang, Z. Janus Nanodisc of Diblock Copolymers. *Adv. Mater.* **2014**, *26*, 4469–4472.

(69) Walther, A.; Matussek, K.; Müller, A. H. E. Engineering Nanostructured Polymer Blends with Controlled Nanoparticle Location Using Janus Particles. *ACS Nano* **2008**, *2*, 1167–1178.

(70) Walther, A.; Hoffmann, M.; Müller, A. H. E. Emulsion Polymerization Using Janus Particles as Stabilizers. *Angew. Chemie Int. Ed.* **2008**, *47*, 711–714.

(71) Bahrami, R.; Löbling, T. I.; Gröschel, A. H.; Schmalz, H.; Müller, A. H. E.; Altstädt, V. The Impact of Janus Nanoparticles on the Compatibilization of Immiscible Polymer Blends under Technologically Relevant Conditions. *ACS Nano* **2014**, *8*, 10048–10056.

(72) Gröschel, A. H.; Löbling, T. I.; Petrov, P. D.; Müllner, M.; Kuttner, C.; Wieberger, F.; Müller, A. H. E. Janus Micelles as Effective Supracolloidal Dispersants for Carbon Nanotubes. *Angew. Chemie Int. Ed.* **2013**, *52*, 3602–3606.

(73) Auschra, C.; Stadler, R. Synthesis of Block Copolymers with Poly(Methyl Methacrylate): P(B-b-MMA), P(EB-b-MMA), P(S-b-B-b-MMA) and P(S-b-EB-b-MMA). *Polym. Bull.* **1993**, *30*, 257–264.

(74) Schindelin, J.; Arganda-Carreras, I.; Frise, E.; Kaynig, V.; Longair, M.; Pietzsch, T.; Preibisch, S.; Rueden, C.; Saalfeld, S.; Schmid, B.; Tinevez, J.-Y.; White, D. J.; Hartenstein, V.; Eliceiri, K.; Tomancak, P.; Cardona, A. Fiji: An Open-Source Platform for Biological-

Image Analysis. *Nat. Methods* **2012**, *9*, 676–682.

(75) Pettersen, E. F.; Goddard, T. D.; Huang, C. C.; Couch, G. S.; Greenblatt, D. M.; Meng, E. C.; Ferrin, T. E. UCSF Chimera - A Visualization System for Exploratory Research and Analysis. *J. Comput. Chem.* **2004**, *25*, 1605–1612.

TOC graphic

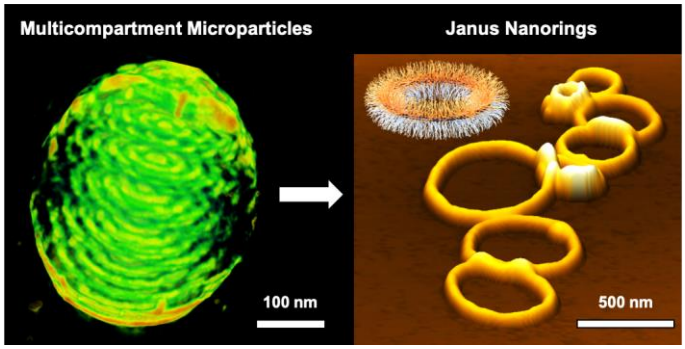
Multicompartment Microparticles
Janus Nanorings
100 nm
500 nm